Taylor & Francis
Taylor & Francis Group

OPEN ACCESS | Check for updates

Multivalent IgM scaffold enhances the therapeutic potential of variant-agnostic ACE2 decoys against SARS-CoV-2

Meghan M. Verstraete [ID][a]*, Florian Heinkel [ID][a]*, Janessa Li[a], Siran Cao[a], Anh Tran [ID][b], Elizabeth C. Halverson[a], Robert Gene[a], Elizabeth Stangle[a], Begonia Silva-Moreno[a], Sifa Arrafi[a], Jegarubee Bavananthasivam [ID][b], Madeline Fung[a], Mariam Eji-Lasisi[a], Stephanie Masterman[a], Steve Xanthoudakis[a], Surjit Dixit[a], John Babcook[a], Brandon Clavette[a], Mark Fogg[a], and Eric Escobar-Cabrera [ID][a]

[a]Zymeworks Inc, Vancouver, Canada; [b]Department of Human Health Therapeutics, National Research Council Canada, Ottawa, Canada

ABSTRACT

As immunological selection for escape mutants continues to give rise to future SARS-CoV-2 variants, novel universal therapeutic strategies against ACE2-dependent viruses are needed. Here we present an IgM-based decavalent ACE2 decoy that has variant-agnostic efficacy. In immuno-, pseudovirus, and live virus assays, IgM ACE2 decoy had potency comparable or superior to leading SARS-CoV-2 IgG-based mAb therapeutics evaluated in the clinic, which were variant-sensitive in their potency. We found that increased ACE2 valency translated into increased apparent affinity for spike protein and superior potency in biological assays when decavalent IgM ACE2 was compared to tetravalent, bivalent, and monovalent ACE2 decoys. Furthermore, a single intranasal dose of IgM ACE2 decoy at 1 mg/kg conferred therapeutic benefit against SARS-CoV-2 Delta variant infection in a hamster model. Taken together, this engineered IgM ACE2 decoy represents a SARS-CoV-2 variant-agnostic therapeutic that leverages avidity to drive enhanced target binding, viral neutralization, and *in vivo* respiratory protection against SARS-CoV-2.

Introduction

As of May 2023, SARS-CoV-2, the causative agent of COVID-19, accounted for more than 766 million confirmed infections and 6.93 million reported deaths worldwide.[1] Even in the face of an armamentarium of countermeasures, including non-pharmaceutical interventions, therapeutic monoclonal antibodies (mAbs), antivirals, and multiple effective vaccines, SARS-CoV-2 has sustained prevalence in the human population. Efforts to curtail the pandemic have been jeopardized by the rapid evolution and emergence of new strains that can evade therapeutic mAbs and immunity gained by vaccination or natural infection.[2–6]

High levels of transmission in most countries have afforded SARS-CoV-2 the opportunity to explore a large evolutionary space. The receptor-binding domain (RBD) of the spike protein of SARS-CoV-2 has been a region of rapid antigenic evolution and is highly divergent between SARS-CoV-2 variants. The RBD mediates binding to host-cell surface receptor angiotensin-converting enzyme 2 (ACE2) to initiate viral entry and subsequent viral replication.[7,8] Although the human immune response can produce antibodies that target diverse viral surface protein epitopes,[9] in the case of SARS-CoV-2, a large fraction of the neutralizing activity of polyclonal antibody response targets the surface-exposed spike protein RBD.[10–12] Since antibodies capable of blocking this RBD-ACE2 interaction can inhibit viral infection, the majority of vaccine strategies use the spike protein to induce immunity,[13,14] and similarly, seven of the eight authorized or approved anti-SARS-CoV-2 therapeutic mAbs target the RBD.[15,16] Hence, mutations that affect the antigenicity of the spike protein, specifically at the RBD-ACE2 interface, can potently diminish neutralization by both therapeutic mAbs and antibodies elicited by previous SARS-CoV-2 infection or vaccination.[12,17–20]

In response to the changing immune profile of the human population, a real-time evolutionary arms race has transpired between SARS-CoV-2 and host. The recent rise of the SARS-CoV-2 Omicron (B.1.1.529) strain and its subvariants (BA.1, BA.2, BA.3, BA.2.12.1, BA.2.13, BA.4, and BA.5) has underscored how mutations affecting the antigenic phenotype have led to failure of all mAbs granted an emergency use authorization (EUA) in the United States and evasion of humoral immunity from natural infection or vaccination.[5,6,21–24] Development of new therapeutic mAbs and updated vaccine sequences, however, is inherently "reactive", typically shows diminished neutralization capacity against emerging variants,[22,25] and relies on continued surveillance of genetic and antigenic changes in the global virus population. Although modeling approaches to predict emerging phenotypic trajectories may be developed, as is the case for influenza virus,[26] prediction of the mutational pathways by which a virus such as SARS-CoV-2 will evolve is extremely challenging and limits the ability to proactively approach the pandemic, as the Omicron variant showed.[27]

Since the interaction between the RBD and the host cell receptor ACE2 is essential for infection, the phenotypic impact of mutations accumulated in the RBD can be avoided by generating an ACE2 based decoy therapeutic.[28] As mutational escape of the SARS-CoV-2 from ACE2 binding for viral attachment and host cell entry would be a considerable evolutionary hurdle, ACE2 decoys could be effective agnostic of mutations accumulated in the spike RBD. This general concept has been tested using monomeric, wildtype (WT) recombinant ACE2 decoy in a Phase 2 trial (NCT04335136). The ACE2 protein was found to be safe and well tolerated, improved mechanical ventilator-free days, and reduced viral loads, but did not reduce mortality. A variety of next-generation ACE2 decoy modalities have been pursued, including dimeric, trimeric, or tetrameric ACE2 decoys using different multivalent scaffolds to achieve avidity mediated affinity enhancements for viral spike protein.[29–32] Although increased efficacy has been achieved relative to monomeric ACE2 decoys, a non-human multivalent scaffold could introduce an immunogenicity risk.[33] Another strategy that has been pursued relies on engineering ACE2 decoys or ACE2-mimic miniproteins to have sub-nanomolar affinity for spike protein.[34–38] These affinity-engineered ACE2 decoy molecules can be broadly neutralizing against different SARS-CoV-2 strains.[33,34] However, the risk of immunogenicity and evolutionary mutational escape remains and could lead to the selection of viral mutants that evade binding affinity-engineered ACE2 decoys, but retain binding to WT, host cell-surface ACE2.

The alternative approach to developing high affinity ACE2 decoys presented here uses multimeric, human IgM as a high-valency scaffold to drive higher apparent affinity binding to spike protein via avidity. By using WT human ACE2 and pentameric IgM as a scaffold, we engineered a decavalent ACE2 decoy which we found to have enhanced viral neutralization properties against all tested variants of concern (VOC) of SARS-CoV-2 as demonstrated *in vitro* by binding, immuno-, pseudovirus-, and live virus assays. In addition, we demonstrate *in vivo* therapeutic benefit of IgM ACE2 decoy relative to bivalent IgG ACE2 decoy molecules in a hamster model of SARS-CoV-2 infection. Our results demonstrate that potency of the IgM-based ACE2 decoy molecule is agnostic of SARS-CoV-2 variant spike protein, in contrast with clinical anti-spike protein mAb benchmarks tested. A high valency, avidity-driven WT ACE2 decoy could serve as a proactive approach to treat future emergent strains of SARS-CoV-2 or any other virus that uses ACE2 as entry point, providing a variant agnostic solution to the SARS-CoV-2 driven pandemic with minimal risk of evolutionary escape.[39]

Results

Increasing ACE2 valency in ACE2 decoys increases binding avidity to spike protein

Preserving the WT, human ACE2 sequence was made paramount in the design of the ACE2 decoys presented here to retain the WT-like binding interface with SARS-CoV-2 spike protein, reduce the risk of immunogenicity, and mitigate risk of viral evolutionary escape. As an alternative to mutation-based affinity engineering, we designed multivalent ACE2 decoy variants on IgG Fc, IgA Fc, or IgM Fc scaffolds to investigate avidity-mediated increases in affinity. Importantly, the WT, human IgM sequence was used to reduce the risk of immunogenicity. Using heterodimeric IgG OAA (one-armed antibody) and homodimeric IgG scaffolds, as well as exploiting the natural multimerization of IgA (dimeric) and IgM (pentameric) Fc when co-expressed with the J chain, we obtained ACE2 decoys that were monovalent, bivalent, tetravalent, and decavalent for ACE2, respectively (Figure 1a).

The ACE2 decoy constructs described above were assessed for binding to SARS-CoV-2 spike protein by surface plasmon resonance (SPR) and on-cell binding. Binding to SARS-CoV-2 Wuhan (WT) spike protein RBD by SPR revealed that higher ACE2 valency decoys bound with higher apparent affinity (Table 1). Specifically, decavalent IgM ACE2 decoy had the highest affinity with an apparent K_D of 0.097 nM, followed by 0.35 nM for tetravalent IgA ACE2 decoy, 3.4 nM for bivalent IgG ACE2 decoy, and lastly monovalent IgG OAA ACE2 decoy, which bound the weakest with a K_D of 81 nM (Table 1). The affinity measurements for monovalent ACE2 binding to Wuhan (WT) spike RBD were consistent with reported literature values that are in the double digit nanomolar range.[35,40,41] It should be noted that apparent affinities are reported for multivalent ACE2 decoys, as a 1:1 binding model was used to fit the kinetic data. Sensorgrams generated from multivalent interactions are a summation of distinct binding events, so a more complex model would be required to accurately describe the combination of kinetic rate constants for multivalent ACE2 decoy binding to spike RBD.[42] However, complex models require the fitting of multiple variables and often result in highly uncertain values. As the goal was to measure the functional affinity due to avidity effects to distinguish between monovalent and avidity-enhanced interactions, the 1:1 binding model was sufficient to rank order ACE2 decoy molecule binding using apparent K_D values as a measure of avidity. The sensorgrams in Figure 1b and S1 illustrate the avidity gain conferred by higher valency IgA and IgM ACE2 decoys based on the decreased off-rate relative to monovalent IgG OAA ACE2 decoy.

ACE2 decoy binding was also measured for SARS-CoV-2 Delta (B.1.617.2) and Omicron (B.1.1.529) variant RBDs and apparent affinity correlated with ACE2 valency across the different variants tested (Table 1). For comparison, the binding affinities of casirivimab (REGN10933) and imdevimab (REGN10987), the two anti-spike mAbs used in Regeneron's REGEN-COV cocktail that was previously granted an EUA, were measured for the same suite of SARS-CoV-2 variant RBDs. Both antibodies bound to SARS-CoV-2 Wuhan (WT) and Delta (B.1.617.2) spike RBDs with sub-nanomolar affinities, similar to the apparent affinity measured for IgM ACE2 (Table 1). In contrast, REGEN-COV mAb imdevimab suffered complete loss in binding to SARS-CoV-2 Omicron (B.1.1.529) spike RBD and the K_D of casirivimab was 1.2 μM, while IgM ACE2 decoy retained high apparent affinity of 2.4 nM (Table 1). Consistent with our design strategy, decavalent binding of IgM ACE2 decoy increased the apparent affinity to spike RBD by two orders of magnitude relative to
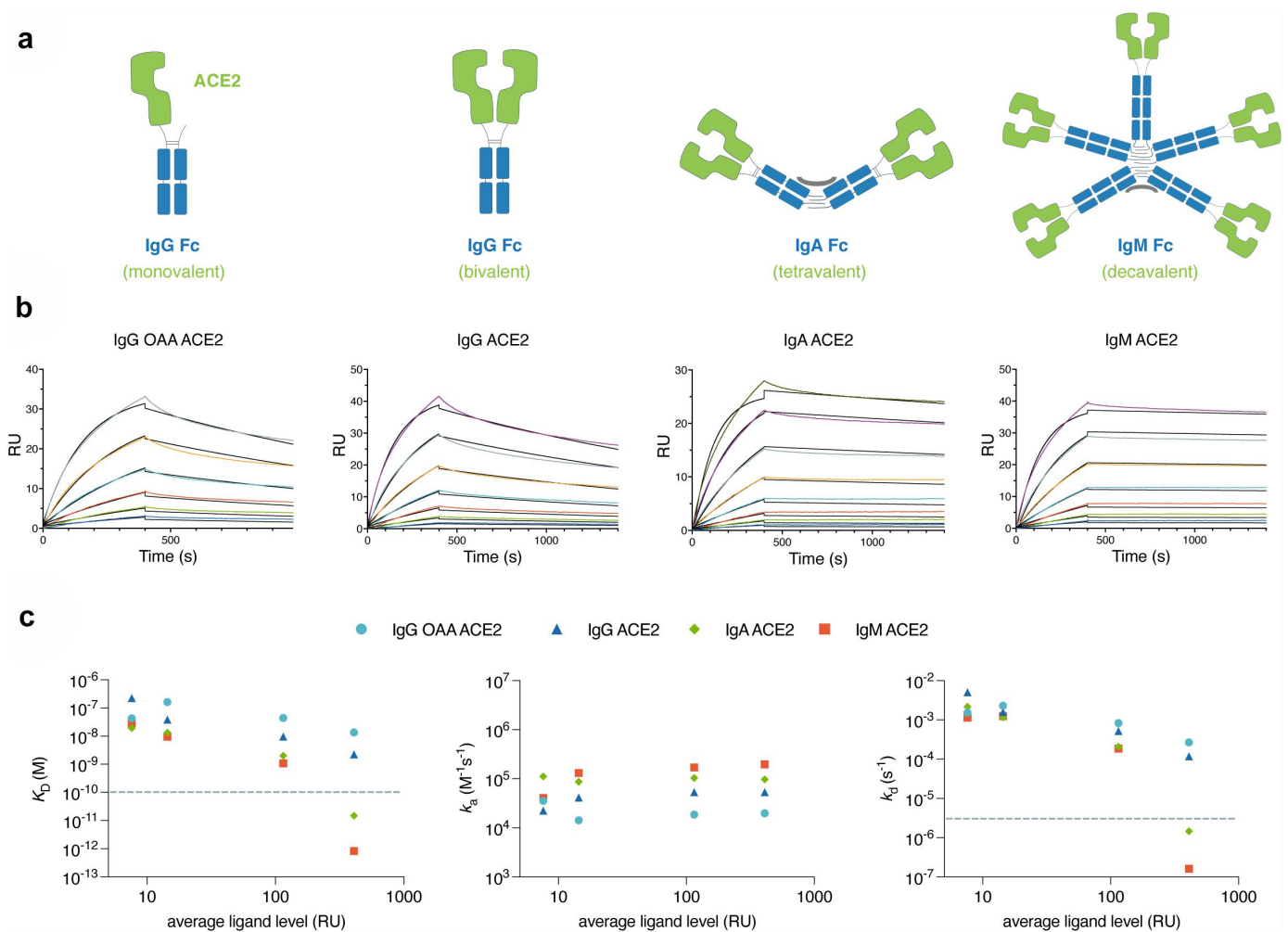
Figure 1. Avidity-driven binding of ACE2 decoys to SARS-CoV-2 Wuhan (WT) strain spike RBD increases with higher ACE2 valency. (a) Depicted left to right is monovalent IgG OAA ACE2 decoy, bivalent IgG ACE2 decoy, tetravalent IgA ACE2 decoy, and decavalent IgM ACE2 decoy with the Fc scaffold colored blue and ACE2 shown in green. (b) SARS-CoV-2 Wuhan (WT) spike protein RBD binding sensorgrams for (left to right) IgG OAA, IgG, IgA, and IgM ACE2 decoys measured by SPR where spike protein was immobilized (~100 RU) on the sensor chip. The sensorgrams illustrate the avidity gain afforded by multivalent ACE2 scaffold based on the decreasing off-rate with increasing ACE2 valency. (c) Multivalent ACE2 decoys bind SARS-CoV-2 spike protein RBD with higher avidity as sensor chip surface Wuhan (WT) spike RBD ligand level increases. (left) The apparent K_D of multivalent ACE2 decoys measured for different RBD ligand densities shows the effect of avidity as increasing concentrations of immobilized spike RBD results in tighter binding. The K_D of monovalent IgG OAA ACE2 decoy did not change significantly with changing RBD ligand density. The association (k_a; middle) and dissociation (k_d; right) rates measured are plotted against the different immobilized RBD ligand densities. The dashed limit represents the LOD. Apparent K_D values are reported for multivalent ACE2 decoys as binding curves are fit by 1:1 kinetic model.

monovalent IgG OAA ACE2 decoy agnostic of SARS-CoV-2 variant RBD tested (Table S1).

To ascertain if increasing apparent affinity measured for higher valency ACE2 decoys was due to a gain in avidity, binding kinetics to SARS-CoV-2 Wuhan (WT) RBD immobilized at different ligand densities on the sensorchip surface were measured. All multivalent ACE2 decoys had further increased apparent affinities at higher immobilization levels of spike RBD due to decreasing off-rates, indicating the contribution of avidity (Figure 1c). In contrast, the monovalent IgG OAA ACE2 decoy did not show the same degree of affinity enhancement as multivalent ACE2 decoys with increased ligand density due to the theoretical independence of 1:1 binding kinetics to ligand concentrations (Figure 1c).

On-cell binding of our panel of ACE2 decoys to SARS-CoV-2 Wuhan (WT) spike protein transfected mammalian cells was also measured and found to have the same rank order in apparent affinity as determined by SPR (Figure S2).

Mammalian cells were transfected with the plasmid encoding the full-length SARS-CoV-2 Wuhan strain spike protein, resulting in cell surface expression of trimeric spike protein. For this experiment, ACE2 decoys designed with a single C-terminal myc-tag were used such that the same anti-myc secondary antibody could be used to detect IgG, IgA, and IgM ACE2 decoys. Lower B_{max} was observed for the higher valency ACE2 decoys, indicating that fewer molecules are required to saturate all on-cell binding sites consistent with a mechanism of multivalent binding to surface spike protein RBDs.

IgM ACE2 decoy shows enhanced potency for disrupting ACE2:spike protein interaction compared to decoys with lower ACE2 valency and is effective agnostic of SARS-CoV-2 variant tested

To determine if the high, avidity-driven binding measured for IgM ACE2 decoy translated to improved neutralization

Table 1. Binding kinetics of ACE2 decoy variants and clinical comparators to recombinant spike protein RBD as measured by SPR.

SARS-CoV-2 strain	Wuhan (WT)			Delta (B.1.617.2)			Omicron (B.1.1.529)		
	k_a (M^{-1} s^{-1})	k_d (s^{-1})	K_D (M)[a]	k_a (M^{-1} s^{-1})	k_d (s^{-1})	K_D (M)[a]	k_a (M^{-1} s^{-1})	k_d (s^{-1})	K_D (M)[a]
IgM ACE2	3.8E + 05	3.5E−05	9.7E−11	2.6E + 05	1.3E−04	4.9E−10	1.5E + 05	3.6E−04	2.4E−09
IgA ACE2	1.8E + 05	9.9E−05	3.5E−10	1.5E + 05	2.2E−04	8.0E−10	2.1E + 05	5.7E−04	2.7E−09
IgG ACE2	1.2E + 05	4.0E−04	3.4E−09	8.5E + 04	5.1E−04	6.0E−09	5.0E + 04	1.2E−03	2.3E−08
IgG OAA- ACE2	1.0E + 05	5.5E−04	8.1E−09	8.3E + 04	6.3E−04	1.1E−08	1.3E + 04	1.7E−03	1.3E−07
Casirivimab	3.0E + 06	2.1E−04	7.1E−11	2.9E + 06	2.0E−04	7.0E−11	N/A[b]	N/A[b]	1.2E−06[b]
Imdevimab	3.4E + 06	2.9E−04	8.7E−11	2.6E + 06	2.8E−04	1.1E−10	no binding		
IgM isotype control	no binding			no binding			no binding		
IgG isotype control	no binding			no binding			no binding		

[a]Kinetic values derived using a 1:1 model and reported as apparent K_D values for multivalent molecules.
[b]K_D value determined using steady state affinity analysis thus N/A indicated for k_a and k_d values.

efficacy, we performed a number of *in vitro* assays to assess the ability of ACE2 decoys to disrupt the SARS-CoV-2 spike:ACE2 interaction. These included neutralization assays using a multiplexed, electrochemiluminescence-based immunoassay from Meso Scale Diagnostics (MSD), pseudotyped lentivirus, and live SARS-CoV-2 virus. The ACE2 decoy molecules were compared against REGEN-COV antibodies either in equimolar combination (1:1) or independently. Bamlanivimab, etesevimab, and sotrovimab were also assessed in a number of assays (Table S1).

ACE2 decoy variants assessed in multiplex immunoassays (MSD V-PLEX COVID-19 ACE2 Neutralization Kits) were able to compete with recombinant ACE2 for interaction with plate-bound spike protein from different SARS-CoV-2 strains (Figures 2a, S2, S3). IgM ACE2 decoy had the highest potency with half-maximal inhibitory concentration (IC50) ranging between 0.23–0.47 nM across all variant spike proteins, followed by IgA, IgG, and IgG OAA ACE2 decoys which were on average reduced in potency by 3-fold, 5-fold, and 15-fold, respectively (Figure 2d, Table S1, S2). This potency rank order was consistent with SPR and on-cell binding measurements supporting the notion that higher ACE2 valency affords avidity that can drive high affinity binding and potentially increase viral neutralization efficacy. Additionally, each
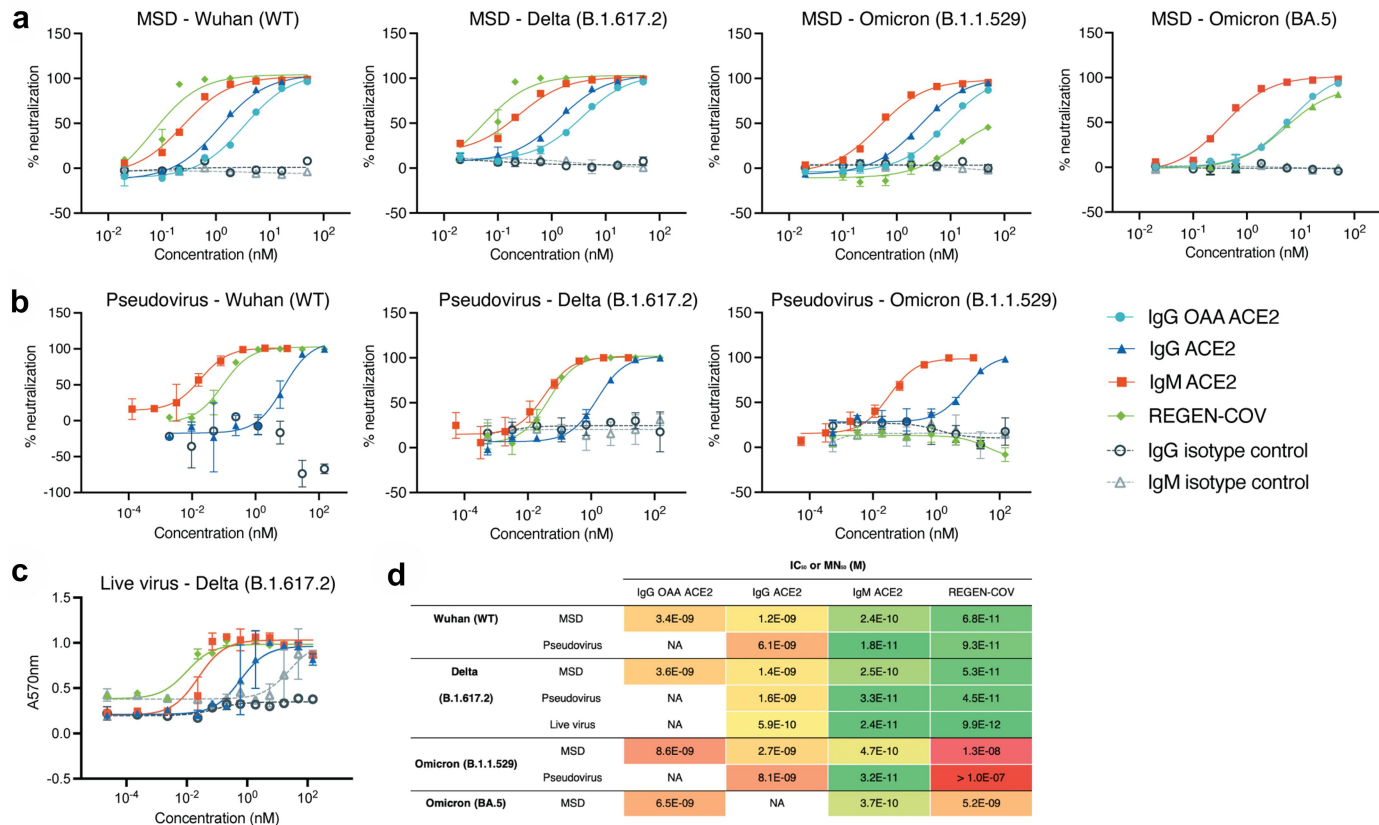

Figure 2. Neutralization of SARS-CoV-2 variant spike protein and ACE2 binding by ACE2 decoys and REGEN-COV mAb cocktail by blocking immunoassay, pseudovirus, and live virus neutralization assays. (a) MSD immunoassay of SARS-CoV-2 Wuhan (WT), Delta (B.1.617.2), and Omicron (B.1.1.529) spike protein binding to SULFO-tagged ACE2. (b) Neutralization of SARS-CoV-2 pseudovirus displaying Wuhan (WT), Delta (B.1.617.2), or Omicron (B.1.1.529) spike proteins from entering ACE2 expressing Opti-HEK293 cells. REGEN-COV cocktail was composed of a 1:1 combination of casirivimab and imdevimab each added at the concentration indicated. (c) Live virus neutralization assay to block SARS-CoV-2 Delta (B.1.617.2) infection of ACE2 expressing Calu-3 cells. Calu-3 cells were stained with crystal violet and viability was determined by measuring absorbance at 570 nm. (d) Table summarizing the IC$_{50}$ (MSD immunoassay and pseudovirus neutralization) and MN$_{50}$ (live virus neutralization) values calculated for ACE2 decoys and REGEN-COV in each assay.

ACE2 decoy retained similar potency across all SARS-CoV-2 variant spike proteins tested. In contrast, numerous clinically relevant anti-spike benchmark antibodies showed SARS-CoV-2 variant-dependent potency (Figures 2a, S2, S4). Notably, IC50s for REGEN-COV against Wuhan (WT), Alpha (B.1.1.7), Beta (B.1.351), Gamma (P.1), and Delta (B.1.617.2) SARS-COV-2 spike protein ranged from 0.053 nM to 0.40 nM, but decreased against Omicron strains B.1.1.529 and BA.5 to 13 nM and 5.2 nM, respectively (Figure 2d, Table S1). Multiplex immunoassays were also performed with plate-bound spike RBD protein from the various SARS-CoV-2 strains (Table S3). Analysis of ACE2 decoy potency data across spike RBD and trimeric spike protein is correlative with Spearman's correlation r and p values of 0.6989 and <0.0001, respectively, and supports that ACE2 decoy efficacy is maintained against monomeric spike RBD and the trimeric form of the spike protein (Figure S5).

Next, we assessed whether the broad activity of ACE2 decoys against SARS-CoV-2 variants seen in binding and MSD immunoassays translated into blocking infection of an ACE2-expressing cell line by SARS-CoV-2 spike protein pseudotyped lentivirus (Figures 2b, S6, S7). As seen in binding and MSD immunoassays described above, ACE2 valency-dependent and SARS-CoV-2 variant-agnostic efficacy was observed for the ACE2 decoys in pseudovirus neutralization (Figures 2b, S6, S7). IgM ACE2 decoy markedly shifted the neutralization potency relative to molar-matched bivalent IgG ACE2 by an average of 185-fold for lentivirus pseudotyped with Wuhan (WT), Delta (B.1.617.2), Omicron (B.1.1.529), Alpha (B.1.1.7), or Beta (B.1.351) spike protein (Figure 2d, Table S1). Notably, IgM ACE2 decoy and REGEN-COV had neutralization potencies against Wuhan (WT) and Delta (B.1.617.2) pseudovirus within the same order of magnitude, but strikingly, REGEN-COV failed to prevent Omicron

(B.1.1.529) pseudotyped lentivirus from infecting ACE2-expressing cells.

Lastly, the ACE2 decoy variants were tested in a live-virus neutralization assay for their ability to prevent SARS-CoV-2 Delta (B.1.617.2) or Beta (B.1.351) strains from infecting ACE2 positive human lung epithelial Calu-3 cells (Figures 2c, S8). The potency rank order of ACE2 decoys was preserved compared to SPR binding, MSD immunoassay, and pseudovirus neutralization assays. IgM ACE2 decoy had 22-fold enhanced SARS-CoV-2 Delta (B.1.617.2) neutralizing activity compared to bivalent IgG ACE2 decoy (Figure 2d). Furthermore, IgM-based ACE2 decoy molecules showed consistent efficacy between viral strains tested with IC50 values between 0.0084–0.024 nM that was similar to clinical benchmark REGEN-COV which had IC50 values of 0.0099–0.012 nM (Figures 2b, S8, Table S1).

Intranasal delivery of IgM ACE2 decoy confers protection against SARS-CoV-2 Delta (B.1.617.2) variant

To determine the potential of the IgM ACE2 decoy to be used as a respiratory tract-delivered therapeutic, we used a Syrian hamster model of SARS-CoV-2 infection. In this non-lethal model, SARS-CoV-2 can replicate to high titers in the respiratory organs and parameters such as body weight changes and viral genomic RNA in the airways can be used to evaluate virus pathogenicity and the efficacy of therapeutic measures.[43] In this experiment, animals were infected with 8×10^3 plaque-forming units (PFU)/animal SARS-CoV-2 Delta (B.1.617.2) variant, followed by intranasal (IN) administration of a single therapeutic dose of IgG ACE2 decoy, IgM ACE2 decoy, or isotype control at 0.1, 1, or 10 mg/kg or phosphate-buffered saline (PBS) control 6 hours post viral challenge (Figure 3a).
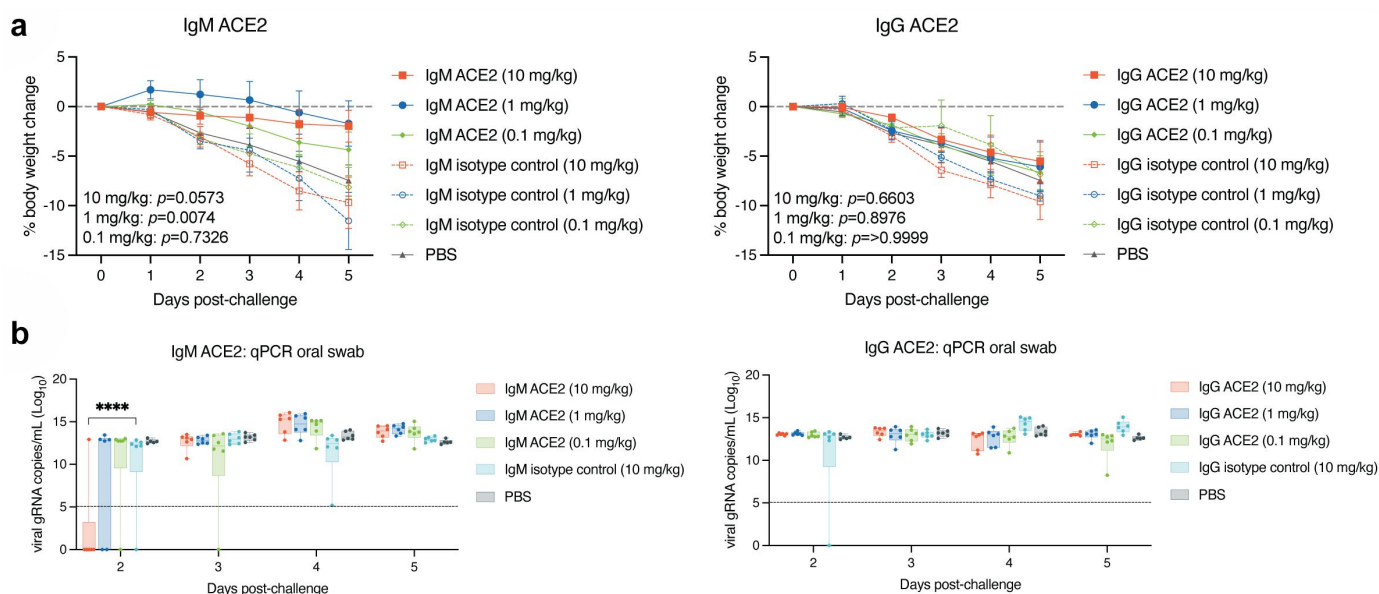

Figure 3. *In vivo* efficacy of intranasal IgM ACE2 decoy and IgG ACE2 decoy for treatment of SARS-CoV-2 Delta (B.1.617.2) infection in a Syrian hamster model. (a) Impact of intranasal treatment with IgM ACE2 or IgG ACE2 decoy on body weight change after viral challenge. P values indicated are based on statistical difference between treatment groups and dose-matched isotype controls on day 5. Error bars represent standard error of the mean. (b) Impact of ACE2 decoy treatment on viral RNA quantified from hamster oral swabs at days 2, 3, 4, and 5 post-challenge (**** indicates significant differences with $p < 0.0001$). Data is plotted as box-and-whisker plot and the dotted line represents the limit of detection (LOD = 5 viral gRNA copies/ml (Log_{10})).

IgM ACE2 decoy showed the greatest protection in challenged animals. Infected hamsters therapeutically treated with IgM ACE2 decoy at 1 mg/kg showed weight gain within the first 72 hrs, while treatment with 10 mg/kg resulted in less than 2% weight change over 5 days post-infection (dpi) (Figure 3a). In contrast, the IgM isotype (10 mg/kg) and PBS controls resulted in weight losses of 10% and 7%, respectively, by 5 dpi. This protection was accompanied by a significant reduction in viral genomic RNA in oral swabs taken on day 2 post viral challenge for hamsters treated with 10 mg/kg IgM ACE2 compared to dose-matched IgM isotype control (Figure 3b). From 3 dpi onwards, viral genomic RNA in oral swabs from hamsters treated with 10 mg/kg IgM ACE2 returned to levels equivalent to dose-matched isotype control (Figure 3b) and hamster body weight started to decline in all treatment groups by 4 and 5 dpi (Figure 3a). The level of live virus quantified from the lung tissue and bronchoalveolar lavage (BAL) at 5 dpi showed little difference to the controls (Figure S9A). A positive weight change is inversely correlated with a reduction in viral burden.[44] This indicates that while IgM ACE2 decoy is effective in reducing both weight loss and viral burden within the first few days after treatment, a single administration was not enough to completely nullify the infection. The increase in viral burden and concurrent decline in animal weight is suggestive of virus rebound with the decline in drug. Therefore, further studies will be needed to determine additional therapeutic doses required to effectively control disease progression and prevent virus rebound.

Histopathological analysis of lung tissues from hamsters infected with SARS-CoV-2 Delta (B.1.617.2) and treated therapeutically with either 10 mg/kg IgM ACE2 or dose-matched IgM isotype control at 5 dpi revealed cellular and morphologic pulmonary alterations consistent with the hamster COVID-19 model. All animals had evidence of viral cytopathic effect and the presence of airway inflammation, alveolar edema, and lymphocyte infiltration. These patterns are all highly characteristic of SARS-CoV-2-induced pneumonia in hamsters.[45,46] No statistically significant histopathological differences between IgM ACE2 decoys and dose-matched isotype controls were observed, which is consistent with live virus quantification at 5 dpi. Although not statistically significant, the percentage of lung section involved and severity of pathologies trended lower in IgM-ACE2 treated hamsters compared to dose-matched IgM isotype control at 10 mg/kg (Figure S9B, C). Visually, the degree of pulmonary consolidation observed between lung images was lower in hamsters treated with IgM ACE2 compared to IgM isotype control at 10 mg/kg (Figure S9D).

In contrast, IgG ACE2 decoy dosed equivalently did not afford the same protection as IgM ACE2 based on prevention of hamster weight loss or reduction in viral genomic RNA in oral swabs at equivalent 1 and 10 mg/kg doses tested relative to dose-matched IgG isotype control (Figure 3a,b). These findings demonstrate the necessity of the ACE2 multivalency afforded by the IgM scaffold in potentiating protective efficacy of the IgM ACE2 decoy.

Discussion

As the probability of immunological selection for escape mutants and continued emergence of antigenically different variants is high, new therapeutic strategies to combat prevailing SARS-CoV-2 variants that are less susceptible to becoming obsolete are needed. In this study we engineered a decavalent IgM-based ACE2 decoy that demonstrates variant-agnostic efficacy at potencies comparable to leading clinical mAb therapeutics when tested in immuno-, pseudovirus, and live virus assays. Based on the consistent potency observed across the different spike variants, we would anticipate that an IgM-ACE2 decoy molecule would be effective against any SARS-CoV-2 variant as long as it retains reliance on ACE2 for viral entry and subsequent infection. Furthermore, we measured increased contributions of avidity to binding of viral spike protein for decoys with increasing ACE2 valency, which translated into superior efficacy in biological assays for decavalent IgM-ACE2 compared to tetravalent, bivalent, and monovalent ACE2 decoys. The superiority of IgM ACE2 decoys in neutralization assays was also reported very recently, although the translation of such effect was not tested *in vivo*.[47]

The concept of using ACE2 as a therapeutic was first propelled by Apeiron Biologics which developed recombinant ACE2, APN01 (GSK2586881), in response to the SARS outbreak in 2003.[48] Application of recombinant ACE2 (APN01) for treatment of SARS-CoV-2 has since been revisited by the company. Recombinant ACE2 theoretically has two mechanisms of action, one to serve as a decoy receptor for viral spike protein[49] and second to attenuate pathology from SARS-CoV-2-induced hyperactivated renin-angiotensin system (RAS) through function of ACE2 catalytic activity.[50] ACE2 is a negative regulator of RAS, and through catalytic cleavage of angiotensin I and II to angiotensin-(1–7) has vasodilatory, antiproliferative, antiangiogenic, and anti-inflammatory properties.[51,52] The COVID-19 Phase 2 clinical trial (NCT04335136) demonstrated that treatment with APN01 was safe and that patients showed improvement on several clinical parameters, but it failed to meet clinical endpoints.[49,53] We speculate that this could have at least in part been due to the relatively low affinity of monomeric ACE2 for spike protein (15–44 nM)[35,40,41] and the intravenous (IV) route for administration used in the trial.

Though most biologics granted an EUA for the treatment of SARS-CoV-2 were administered IV, circulating IgGs mAbs lack efficient access to mucosal surfaces and must be dosed at appreciable concentrations to elicit an effect.[54] Despite these high doses, the resulting amount of mAb that reaches the lungs is still low compared to circulation and suboptimal as a therapeutic dose.[49–52] As the respiratory tract is the major target and site of viral replication for SARS-CoV-2,[55] an alternative strategy to modulating progression of COVID-19 may be through early administration by IN delivery to confer protection against respiratory infection. IN administration can be used to non-invasively deliver higher concentrations of antibody therapeutic directly to the airway tissues and better target the site of virus replication in the respiratory tract.[56–58]

This dose-sparing effect of localized IN application of therapeutic proteins for SARS-CoV-2 has previously been demonstrated in Syrian hamsters and cynomolgus macaques.[59–62]

As such, we designed our *in vivo* study to test therapeutic IN delivery in hamster model of SARS-CoV-2 infection. The results hint at the therapeutic potential of IgM ACE2 decoy based on decreased weight loss relative to isotype control doses at 1 and 10 mg/kg, even though statistically significant therapeutic efficacy was not reached based on body weight loss or decreases in viral titer over the course of the study (Figure 3). However, there was statistically significant decrease in viral genomic RNA at day 2 for IgM ACE2 dosed at 10 mg/kg compared to dose-matched IgM isotype control. The activity of the IgM ACE2 decoy is limited to the apical surface of the epithelial airway; therefore, it is a greater challenge to therapeutically neutralize viral infection with a single dose delivered post-infection. Viruses that have already infected cells will escape the ACE2 decoy and continue to produce progeny virions.[63] This resulted in a rebound of virus infection observed at days 3, 4, and 5 with return of weight loss and increased viral burden after a single dose treatment.

The rebound in virus replication might explain the lack of statistically different lung histopathology in hamsters treated with IgM ACE2. Virus rebound is an issue when insufficient drug is administered, and has been reported for antiretroviral therapies in HIV patients[64] and Paxlovid in SARS-CoV-2 patients.[65,66] This demonstrates the challenge to manage viral infection with a single, therapeutic dose administered after the infection is established in the patient. We hypothesize that additional doses of IgM ACE2 will further neutralize subsequent waves of progeny virion release and provide stronger protection. The data acquired in this *in vivo* study is rather consistent with efficacy data collected on IN delivery of the Regeneron cocktail, REGEN-COV, in a hamster model where prophylactic dosing of mAbs resulted in marked efficacy over isotype control compared to equivalent therapeutic dose post viral challenge.[67] As viral replication and lung pathology change very rapidly in the hamster model, demonstrating therapeutic efficacy with a single treatment post-challenge represents a high bar.[67] Future work to determine the optimal dosing regimen would be informative on the therapeutic benefit that can be achieved using IgM ACE2 decoy.

Co-opting the multivalency afforded by IgM has previously been applied by IGM Biosciences. IgM-6268 is a pentameric IgM antibody with 10 antigen-binding Fab regions against SARS-CoV-2 spike RBD that similarly demonstrates enhanced target binding due to avidity and potency in neutralizing SARS-CoV-2 relative to the paratope-matched, parental bivalent IgG.[58] *In vivo* data also shows efficacious viral neutralization in a mouse model of SARS-CoV-2 infection if the IgM antibody is dosed IN either prophylactically or therapeutically post viral challenge and displayed desirable biodistribution, pharmacokinetic, and safety profiles in rodent models.[58] IgM-6268 has recently advanced to Phase 1 clinical trials to assess safety, tolerability, and pharmacokinetics of IN and intraorally delivered IgM-6268 in healthy volunteers and patients with mild-to-moderate COVID-19 (NCT05160402). Though the efficacy of IgM-6268 in treatment of COVID-19 has not yet been published, a noteworthy observation from the

Phase 1 trial is the low dose range (1–7.5 mg per patient) tested via IN or intraoral administration. This is in stark contrast with the up to 1200 mg IV therapeutic dose used for the Regeneron cocktail (REGEN-COV) of casirivimab (REGN10933) and imdevimab (REGN10987) (www.fda.gov/media/145611/download). The advancement of IgM-6268 molecule into clinical trials using IN delivery shows promise for the development of an IN-delivered IgM-ACE2 decoy therapeutic.

IgM molecules are generally perceived as being difficult to manufacture due to their large size and chemical sensitivities that must be accommodated. However, IgM has a range of characteristics that can support the development of effective purification strategies that avoid unnecessary stress. Recent improvements in cell lines, chromatography methods, and process monitoring have made the production of high-quality IgM more tractable with high yields and safety clearance.[68] Scalable methods relying on multimodal size exclusion of large molecules with concurrent removal of smaller impurities in anionic core and subsequent use of monolithic anion exchange columns ideal for purifying large biomolecules can be developed.[68,69] Here, we used transient transfection for mammalian cell culture expression and a three-step purification method that yielded~25 mg/L of IgM-ACE2. The success displayed by IGM Biosciences to produce IgM-6268 and other IgM-based therapeutics at high titers (>1 g/L)[58] and quantities to support COVID-19 and oncology clinical trials provide evidence that challenges associated with producing IgM-based therapeutics at scale can be overcome.[68]

Additional studies to assess tolerability of IN-administered ACE2-based therapeutics are needed. As discussed above, ACE2 catalytic activity is important in maintaining RAS homeostasis. As seen for APN01, IV-administration of a catalytically active ACE2 decoy provided an additive therapeutic benefit due to its ability to regulate the RAS.[49,52,53] Though it may be hypothesized that a similar clinical benefit could be measured with IN-delivery of IgM ACE2 directly to airway tissues, generating a catalytically inactive version of ACE2 has also been considered to lower risks of toxicity.[70,71] It has previously been demonstrated, however, that mutations in the active site can decrease the thermostability of ACE2, which could potentiate manufacturing or pharmacokinetic liabilities.[72] Nevertheless, ACE2 engineering that preserves the WT RBD-binding ACE2 interface and improves its thermal stability may be considered for future development of an IgM-ACE2 decoy that is catalytically inactive.

In conclusion, we demonstrate that an engineered IgM ACE2 decoy represents a promising SARS-CoV-2 variant-agnostic therapeutic strategy that leverages avidity to drive enhanced target binding, viral neutralization, and *in vivo* respiratory protection against SARS-CoV-2. We hypothesize that, as the WT ACE2-RBD spike protein interface is not engineered, the potential for new viral lineages to become resistant to this drug modality is minimal. Future development of an IN-delivered IgM-ACE2 decoy therapeutic may offer an effective, noninvasive, and flexible therapy that targets airway tissues at the site of viral infection.

Materials and methods

Design and purification of ACE2 decoy variants and controls

ACE2 decoy variants were designed using IgG Fc, IgA Fc, or IgM Fc scaffolds to achieve different valency of ACE2 per molecule. Schematic representations of the ACE2 variant designs are illustrated in Figure 1a. The extracellular domain (domain boundaries Q18-S740 or Q18–D615) of human, WT ACE2 (UniProt accession number: Q9BYF1) was used for the ACE2 decoy variants. For IgM-based ACE2 decoy, WT ACE2 was fused to the N-terminus of the IgM CH2 of the IgM Fc. The IgM tailpiece was also included to enable pentameric multimerization in the presence of the J chain to generate a molecule that is decavalent for ACE2. An IgA-based ACE2 decoy was designed by attaching WT ACE2 to the N-terminus of the IgA2 hinge-IgA1 Fc chimera containing mutation C192S to remove free cysteine responsible for covalent attachment to pIgR. The IgA2 hinge domain boundaries were used as described previously[73] and the IgA tailpiece was left intact to allow dimeric multimerization when co-expressed with the J chain to generate a molecule that is tetravalent for ACE2. IgG-based ACE2 decoys either monovalent or bivalent for ACE2 were also designed. In these, either one or two ACE2 were fused directly to the N-terminus of the IgG1 hinge to generate IgG-based ACE2 decoys. To allow for selective heterodimeric pairing for design of monovalent ACE2 IgG decoy variants, referred throughout as IgG one-armed antibody (OAA) ACE2 decoy, mutations were introduced in the CH3 domains of the IgG Fc as described previously.[74] Mutations L234A, L235A, and D265S were also introduced in both CH2 domains to reduce binding to the Fc gamma receptors. Some variants contained a single G4S linked myc-tag (GGGGSEQKLISEEDL) for detection purposes either by fusion of the myc-tag to the C-terminus of the J chain for IgM and IgA ACE2 decoys or the C-terminus of the IgG Fc. A single myc-tag per IgG ACE2 and IgG OAA ACE2 variants was achieved using mutations introduced in the CH3 domains of the IgG Fc as described previously.[74] Benchmark control antibodies casirivimab (REGN10933), imdevimab (REGN10987), bamlanivimab (LY-COV555), etesevimab (LY-CoV016), and sotrovimab (S309) VH/VL sequences were cloned into an IgG1 framework (mAb VH/VL sequences available in KEGG DRUG Database).

ACE2 decoy variants, isotype control antibodies, and benchmark antibodies were cloned into expression vectors according to standard cloning procedures and expressed in transient mammalian cell culture using Expi293 cells. Co-expression of the ACE2 IgM heavy chain or ACE2 IgA heavy chain with J chain led to covalent assembly of either pentameric IgM molecule or dimeric IgA molecule, respectively. IgG-based molecules were purified using affinity chromatography (MabSelect SuRe, Cytiva), followed by preparative size exclusion chromatography (SEC) (Superdex 200 Increase 10/300 GL, Cytiva). The IgA ACE2 decoy variant was purified using anion exchange chromatography (Foresight Nuvia HP-Q, Bio-Rad Laboratories) followed by a polishing step using ceramic hydroxyapatite chromatography (Foresight CHT II-40, Bio-Rad Laboratories). The IgM ACE2 decoy variant was purified using mixed mode chromatography (Capto Core 700, Cytiva) followed by anion exchange chromatography (CIMmultus QA monolithic column, BIA separations) and preparative SEC (Superose 6 Increase 10/300 GL, Cytiva). Lastly, the purification method for the IgM isotype control used a mixed mode chromatography (Capto Core 400, Cytiva) step followed by anion exchange chromatography (Foresight Nuvia HP-Q, Bio-Rad Laboratories) and a polishing step using hydroxyapatite chromatography (Foresight CHT II-40, Bio-Rad Laboratories). The purified ACE2 variants and isotype controls were all equilibrated in PBS, pH 7.4 and assessed for purity and correct assembly by non-reducing SDS-PAGE (data not shown). IgG molecules were run on 4–15% mini-PROTEAN TGX precast gel (Bio-Rad Laboratories) and IgA/IgM molecules were run on 7.5% mini-PROTEAN TGX precast gel (Bio-Rad Laboratories). The proteins were also assessed by analytical SEC using Acquity BEH SEC column with 200 Å or 450 Å pore size (Waters Corporation) for IgG molecules and IgA/IgM molecules, respectively.

A REGEN-COV mAb cocktail was prepared by mixing casirivimab and imdevimab at 1:1 molar ratio[75] and the Eli Lilly bamlanivimab and etesevimab mAb cocktail by mixing bamlanivimab and etesevimab at 1:2 molar ratio, respectively.[76]

ACE2 decoy binding measurements using SPR

SPR affinity measurements for the ACE2 decoys and controls were performed using a Biacore T200 instrument (Cytiva) at 25°C using HBS EP+ buffer (#BR100669, Cytiva). His-tagged spike RBD proteins for Wuhan (WT) (#10500-CV, R&D Systems), Delta (B.1.617.2) (#10876-CV, R&D Systems), Omicron (B.1.1.529) (#40592-V08H121, Sino Biological), Alpha (B.1.1.7) (#10730-CV, R&D Systems), Beta (B.1.351) (#10735-CV, R&D Systems), and Gamma (P.1) (#10775-CV, R&D Systems) were each covalently immobilized on a CM5 Series S sensor chip by amine coupling to ligand density of ~100 RU. To measure avidity-driven binding of multivalent ACE2 decoys, as a series of captured spike RBD protein levels were generated by covalently immobilizing Wuhan (WT) spike RBD (#10500-CV, R&D Systems on CM5 Series S sensor chip to ligand densities of ~7, 15, 100, and 400 RU. Different ligand densities were achieved by flowing Wuhan (WT) spike RBD at 1.5 µg/ml at 5 µl/min for varying contact times on each flow cell to achieve the target level of ligand density. Nine concentrations following a two-fold dilution series of IgG, IgA, and IgM ACE2 decoy variants, casirivimab, or imdevimab were injected for 400 seconds at a flow rate of 30 µl/min, then were dissociated by running buffer for 600–1800 seconds. 10 mM glycine-HCl pH 2.0 was used to regenerate the surface between each cycle for 30 seconds at 30 µl/min. The binding kinetics were analyzed using the 1:1 binding model and kinetic analyses were performed using Biacore T200 Evaluation Software v3.0.

Generation of transient spike protein expressing HEK293-6E and on-cell binding measurements of ACE2 decoys

HEK293-6E cells were transiently transfected with full-length Wuhan (WT) spike (pCMV3 backbone, Sino Biological, #VG40589-UT) or mock GFP negative control (pD2610-CMV(v23)-GFP). Spike protein expression on transfected HEK293-6E cells was confirmed by flow cytometry using Quantum™ Simply Cellular® anti-Human IgG beads (Bangs Laboratories, #816) and 15 µg/mL anti-spike-AF647 (eBioscience, #51-6490-82) antibody according to the manufacturer's protocol.

Spike[+] HEK293-6E and negative control mock-transfected GFP HEK293 –6E (mock-GFP[+]) were pre-mixed and analyzed by flow cytometry to evaluate the binding of myc-tagged ACE2 decoy variants to ectopically expressed full-length wild type Wuhan SARS-CoV-2 spike protein. In brief, spike[+] and mock-GFP[+] HEK293-6E cells were mixed 1:1 and added to myc-tagged ACE2 decoy variants serially diluted in an 8-point, 3-fold titration curve starting at 50 nM. After incubation for 45 minutes at 4°C, cells were washed then mixed with LIVE/DEAD Fixable Viability dye and anti-MYC secondary antibody (clone 4A6, mouse monoclonal IgG1, Millipore, #05–724-25UG) labeled with Zenon™ Mouse IgG1 Labelling Kit AF647 (Thermo, #Z25008). Samples were incubated with secondary antibody for 45 minutes at room temperature and then plates were washed twice and analyzed on a BD FACSCelesta™ cell analyzer. Data were reported as fold over background (mock-GFP^{+} cells) calculated using formula A indicated below.

Formula A

$$\text{Fold over background} = \frac{\text{AF647 geometric mean spike}^+ \text{ cells}}{\text{AF647 geometric mean mock GFP}^+ \text{ cells}}$$

Spike protein and ACE2 interaction blocking immunoassay

The V-PLEX SARS-CoV-2 Panel 22, 23, 25, and 27 kits (Meso Scale Diagnostics, LLC K15562U, K15570U, K15586U, K15606U) were used to quantitatively measure the ability of ACE2 decoy variants and anti-spike antibodies to block the binding of SULFO-tagged recombinant ACE2 to SARS-CoV-2 variant spike RBD or spike trimeric protein antigens coated on a MULTI-SPOT plate. The assay was performed according to the manufacturer's protocol with an 8-point, 3-fold titration curve of each test article starting at 50 nM. Results are reported as percent neutralization calculated using formula B indicated below.

Formula B

$$\% \text{ neutralization} = \left(1 - \frac{\text{Sample ECL signal}}{\text{Average ECL signal of SULFO tagged ACE2 control}}\right) \times 100\%$$

IC50 values obtained from ACE2 decoy immunoassay neutralization in assays with plates coated with either SARS-CoV-2 variant spike RBD protein or trimeric spike protein were used to determine correlation between the neutralization assays.

Spearman's correlation r and p values were calculated using GraphPad Prism software.

SARS-Cov-2 pseudovirus neutralization assay

A SARS-CoV-2 pseudovirus neutralization assay was used to quantify the inhibition of SARS-CoV-2 pseudotyped lentivirus (pseudovirus) entry into Opti-HEK293/ACE2 cells in the presence of ACE2 decoy variants and anti-spike antibodies. Delta (B.1.617.2) (SC2087W, GenScript) and Omicron (B.1.1.529) (SC2087–027, GenScript) pseudovirus assays were performed by GenScript ProBio (Piscataway, NJ) according to the manufacturer's protocol with a 7-point, 6-fold dilution series starting at 150 nM for all test articles except IgM, which started at 15 nM. Wuhan (WT) pseudovirus assay (SC2087A, GenScript) was performed according to manufacturer's protocol with a 4-fold reduction in volumes to transition from 96-well to 384-well plate format. Test articles were titrated in an 8-point, 4-fold serial dilution series starting from a top concentration of 150 nM (10 nM for IgM) with results reported as percent neutralization calculated using formula C.

Formula C

$$\% \text{ neutralization} = \left(1 - \frac{\begin{array}{c}\text{sample RLU} \\ -\text{average RLU of cells only}\end{array}}{\begin{array}{c}\text{average RLU of cells and virus only} \\ -\text{average RLU of cells only}\end{array}}\right) \times 100\%$$

SARS-CoV-2 live virus neutralization assay

The ability of ACE2 decoy variants and anti-spike antibodies to neutralize SARS-CoV-2 virus (Delta (B.1.617.2) and Beta (B.1.351) variants) infection of Calu-3 cells endogenously expressing ACE2 were assessed by Microbiologics, Inc (St. Cloud, MN). A $TCID_{50}$ (tissue culture infectious dose) end point titer was calculated to determine the viral titer to be used in the neutralization assay. Briefly, 10-fold serial dilutions of both Delta and Beta SARS-CoV-2 variants were incubated with Calu-3 cells and incubated at 37°C in a 5% CO_2 incubator for five days. The virus specific cytopathic effect was observed microscopically for each viral variant and the $TCID_{50}$ was calculated using the Spearman-Karber equation to determine the titer of the virus to be added to the cells. For the live virus neutralization assay, test articles were prepared as a 2× working stock by titrating an 8-point, 3-fold serial dilution followed by a 4-point, 10-fold dilution series starting from 300 nM. Samples were further diluted 1:1 with SARS-CoV-2 Beta or Delta viral stock (approximately 1.0E2 TCID/100 ml) and incubated at 37°C for one hour in a 5% CO_2 incubator. Following the virus and antibody incubation, the sample was transferred to a plate containing Calu-3 cell monolayer and further incubated at 37°C in a 5% CO_2 incubator for five days. Plates were washed, fixed, and stained with crystal violet and the absorbance at 570 nm was measured using Spectramax ID-5 microtiter plate reader. Data were plotted using GraphPad Prism software and fit using sigmoidal, 4PL non-linear equation to determine the MN_{50} (microneutralization concentration).

In vivo SARS-CoV-2 infection and intranasal treatment with ACE2 decoys in hamsters

Male LVG Golden Syrian Hamsters (81–90 g) were obtained from Charles River Laboratories (Saint-Constant, Canada). Animals were maintained at the small animal facility of the National Research Council Canada (NRC) in accordance with the guidelines of the Canadian Council on Animal Care. All procedures performed on animals in this study were approved by the Institutional Review Board (NRC Human Health Therapeutics Animal Care Committee) and covered under animal use protocol 2020.06.

SARS-CoV-2 isolate hCoV-19/USA/MD-HP05647/2021 (Lineage B.1.617.2; Delta variant) was obtained through BEI Resources, NIAID, NIH: NR-55672, contributed by Dr. Andrew S. Pekosz. Virus was propagated on Vero-TMPRSS2 and quantified on Vero cells. Gene sequencing of the spike glycoprotein was carried out to confirm exact genetic identity to the original isolate. Passage 2 virus stocks were used in the in vivo hamster study. All infectious work was carried out under ABSL-3 conditions at the NRC. Animals were randomly allocated into 13 different experimental groups ($n = 6$ animals per group) and were challenged with Delta (B.1.617.2) variant at 8×10^3 PFU/animal. Drugs were administered intranasally at 6 hr post-challenge at 0.1, 1, or 10 mg/kg dosed in 50 µl per nares. Daily weight and clinical scores were determined. Oral swabs were taken daily on days 2 to 5 post infection and transferred directly to 600 µl RNA/DNA Shield (Zymo Research, Irvine, CA). Lung tissue for viral RNA isolation was collected directly into 1 mL RNA/DNA Shield in homogenizer tubes. Viral RNA was extracted under BSL-3 conditions from oral swab samples or mechanically homogenized lung tissues using Quick-RNA Viral Kit (Zymo Research, Irvine, CA).

Viral genomic RNA was quantified by real time-PCR to the target viral envelope gene as previously described.[77] Five days after infection, bronchoalveolar lavage (BAL) and lung tissue necropsy were collected for measurement of infectious viral particles by plaque assay. qRT-PCR was also performed to measure viral RNA in the samples using the method described.[77] Plaque assay was carried out as previously described.[78] In brief, centrifuge clarified supernatant from homogenized lung tissues were diluted in a 1 in 10 serial dilution in infection media. Virus was adsorbed on Vero cells for 1 h at 37°C before inoculum was removed and overlaid with infection media containing 0.6% ultrapure, low-melting point agarose. Infected cells were incubated at 37°C/5% CO_2 for 72 h. After incubation, cells were fixed with 10% formaldehyde and stained with crystal violet. Plaques were enumerated and PFU was determined per gram of lung tissue or per mL of BAL.

An ordinary one-way analysis of variance (ANOVA) was used to compare the percent body weight loss at day 5 between treatment groups and dose-matched isotype control-treated groups. Statistical analysis of viral genomic RNA was conducted using mixed-effects model followed by Tukey's multiple comparisons test. Lastly statistical analysis of BAL and lung viral titers was calculated using ordinary one-way ANOVA. All analyses were performed using GraphPad Prism software (version 9).

Histopathology analysis of hamster lung tissues

Lungs were necropsied from hamsters at 5 days post infection for histopathological analysis. Tissues were fixed in 10% buffered formalin for 24 hrs and processed by standard paraffin embedding methods. Sections (5 µm thick) were mounted onto glass slides and stained with hematoxylin-eosin (HE). Slides were blindly evaluated by a veterinary pathologist (HM) for lung injury using a semiquantitative scoring system. Airway inflammation, alveolar edema, pneumocyte proliferation, alveolar septal edema, alveolar lymphocytes, alveolar eosinophils, alveolar neutrophils, alveolar histiocytes, and viral cytopathic effects were scored on a four-step scale (0 = none, 1 = mild, 2 = moderate, 3 = marked).

Abbreviations

ACE2	receptor angiotensin converting enzyme 2
ANOVA	analysis of variance
BAL	bronchoalveolar lavage
dpi	days post-infection
EUA	Emergency Use Authorization
HE	hematoxylin-eosin
IC50	half-maximal inhibitory concentration
IN	intranasal
IV	intravenous
MN50	half-maximal microneutralization concentration
MSD	Meso Scale Diagnostics
NRC	National Research Council Canada
OAA	one-armed antibody
PFU	plaque-forming units
RAS	renin-angiotensin system
RBD	receptor binding domain
SEC	size exclusion chromatography
SPR	surface plasmon resonance
$TCID_{50}$	tissue culture infectious dose
VOC	variants of concern
WT	wildtype

ORCID

Meghan M. Verstraete http://orcid.org/0000-0003-0422-2826
Florian Heinkel http://orcid.org/0000-0002-2383-9330

Anh Tran http://orcid.org/0000-0003-0644-6014
Jegarubee Bavananthasivam http://orcid.org/0000-0002-0332-4823
Eric Escobar-Cabrera http://orcid.org/0000-0002-2749-8860

References

1. World Health Organization. WHO coronavirus (COVID-19) dashboard; 2023 May 19. https://covid19.who.int/ .
2. Weisblum Y, Schmidt F, Zhang F, DaSilva J, Poston D, Lorenzi JC, Muecksch F, Rutkowska M, Hoffmann HH, Michailidis E, et al. Escape from neutralizing antibodies by SARS-CoV-2 spike protein variants. Elife. 2020;9. doi:10.7554/eLife.61312. PMID: 33112236.
3. Andreano E, Piccini G, Licastro D, Casalino L, Johnson NV, Paciello I, Dal Monego S, Pantano E, Manganaro N, Manenti A, et al. SARS-CoV-2 escape from a highly neutralizing COVID-19 convalescent plasma. Proc Natl Acad Sci U S A. 2021;118(36):118. doi:10.1073/pnas.2103154118. PMID: 34417349.
4. McCarthy KR, Rennick LJ, Nambulli S, Robinson-McCarthy LR, Bain WG, Haidar G, Duprex WP. Recurrent deletions in the SARS-CoV-2 spike glycoprotein drive antibody escape. Science. 2021;371(6534):1139–42. doi:10.1126/science.abf6950. PMID: 33536258.
5. Yamasoba D, Kosugi Y, Kimura I, Fujita S, Uriu K, Ito J, Sato K, Genotype to Phenotype Japan C. Neutralisation sensitivity of SARS-CoV-2 omicron subvariants to therapeutic monoclonal antibodies. Lancet Infect Dis. 2022;22(7):942–43. doi:10.1016/S1473-3099(22)00365-6. PMID: 35690075.
6. Cao Y, Yisimayi A, Jian F, Song W, Xiao T, Wang L, Du S, Wang J, Li Q, Chen X, et al. BA.2.12.1, BA.4 and BA.5 escape antibodies elicited by Omicron infection. Nature. 2022;608(7923):593–602. doi:10.1038/s41586-022-04980-y. PMID: 35714668.
7. Letko M, Marzi A, Munster V. Functional assessment of cell entry and receptor usage for SARS-CoV-2 and other lineage B betacoronaviruses. Nat Microbiol. 2020;5(4):562–69. doi:10.1038/s41564-020-0688-y. PMID: 32094589.
8. Hoffmann M, Kleine-Weber H, Schroeder S, Kruger N, Herrler T, Erichsen S, Schiergens TS, Herrler G, Wu NH, Nitsche A, et al. SARS-CoV-2 cell entry depends on ACE2 and TMPRSS2 and is blocked by a clinically proven protease inhibitor. Cell. 2020;181 (2):271–80 e278. doi:10.1016/j.cell.2020.02.052. PMID: 32142651.
9. Greaney AJ, Starr TN, Barnes CO, Weisblum Y, Schmidt F, Caskey M, Gaebler C, Cho A, Agudelo M, Finkin S, et al. Mapping mutations to the SARS-CoV-2 RBD that escape binding by different classes of antibodies. Nat Commun. 2021;12(1):4196. doi:10.1038/s41467-021-24435-8. PMID: 34234131.
10. Robbiani DF, Gaebler C, Muecksch F, Lorenzi JCC, Wang Z, Cho A, Agudelo M, Barnes CO, Gazumyan A, Finkin S, et al. Convergent antibody responses to SARS-CoV-2 in convalescent individuals. Nature. 2020;584(7821):437–42. doi:10.1038/s41586-020-2456-9. PMID: 32555388.
11. Piccoli L, Park YJ, Tortorici MA, Czudnochowski N, Walls AC, Beltramello M, Silacci-Fregni C, Pinto D, Rosen LE, Bowen JE, et al. Mapping neutralizing and immunodominant sites on the SARS-CoV-2 spike receptor-binding domain by structure-guided high-resolution serology. Cell. 2020;183(4):1024–42 e1021. doi:10.1016/j.cell.2020.09.037. PMID: 32991844.
12. Greaney AJ, Loes AN, Crawford KHD, Starr TN, Malone KD, Chu HY, Bloom JD. Comprehensive mapping of mutations in the SARS-CoV-2 receptor-binding domain that affect recognition by polyclonal human plasma antibodies. Cell Host & Microbe. 2021;29(3):463–76 e466. doi:10.1016/j.chom.2021.02.003. PMID: 33592168.
13. Dai L, Gao GF. Viral targets for vaccines against COVID-19. Nat Rev Immunol. 2021;21(2):73–82. doi:10.1038/s41577-020-00480-0. PMID: 33340022.
14. Sternberg A, Naujokat C. Structural features of coronavirus SARS-CoV-2 spike protein: targets for vaccination. Life Sci. 2020;257:118056. doi:10.1016/j.lfs.2020.118056. PMID: 32645344.
15. Corti D, Purcell LA, Snell G, Veesler D. Tackling COVID-19 with neutralizing monoclonal antibodies. Cell. 2021;184(17):4593–95. doi:10.1016/j.cell.2021.07.027. PMID: 34416148.
16. Cameroni E, Bowen JE, Rosen LE, Saliba C, Zepeda SK, Culap K, Pinto D, VanBlargan LA, De Marco A, di Iulio J, et al. Broadly neutralizing antibodies overcome SARS-CoV-2 omicron antigenic shift. Nature. 2022;602(7898):664–70. doi:10.1038/s41586-021-04386-2. PMID: 35016195.
17. Harvey WT, Carabelli AM, Jackson B, Gupta RK, Thomson EC, Harrison EM, Ludden C, Reeve R, Rambaut A, Consortium CG, et al. SARS-CoV-2 variants, spike mutations and immune escape. Nat Rev Microbiol. 2021;19(7):409–24. doi:10.1038/s41579-021-00573-0. PMID: 34075212.
18. Starr TN, Greaney AJ, Addetia A, Hannon WW, Choudhary MC, Dingens AS, Li JZ, Bloom JD. Prospective mapping of viral mutations that escape antibodies used to treat COVID-19. Sci. 2021;371 (6531):850–54. doi:10.1126/science.abf9302. PMID: 33495308.
19. Liu Z, VanBlargan LA, Bloyet LM, Rothlauf PW, Chen RE, Stumpf S, Zhao H, Errico JM, Theel ES, Liebeskind MJ, et al. Identification of SARS-CoV-2 spike mutations that attenuate monoclonal and serum antibody neutralization. Cell Host & Microbe. 2021;29(3):477–88 e474. doi:10.1016/j.chom.2021.01.014. PMID: 33535027.
20. Li Q, Wu J, Nie J, Zhang L, Hao H, Liu S, Zhao C, Zhang Q, Liu H, Nie L, et al. The impact of mutations in SARS-CoV-2 spike on viral infectivity and antigenicity. Cell. 2020;182(5):1284–94 e1289. doi:10.1016/j.cell.2020.07.012. PMID: 32730807.
21. VanBlargan LA, Errico JM, Halfmann PJ, Zost SJ, Crowe JE Jr., Purcell LA, Kawaoka Y, Corti D, Fremont DH, Diamond MS. An infectious SARS-CoV-2 B.1.1.529 omicron virus escapes neutralization by therapeutic monoclonal antibodies. Nat Med. 2022;28 (3):490–95. doi:10.1038/s41591-021-01678-y. PMID: 35046573.
22. Wang P, Nair MS, Liu L, Iketani S, Luo Y, Guo Y, Wang M, Yu J, Zhang B, Kwong PD, et al. Antibody resistance of SARS-CoV-2 variants B.1.351 and B.1.1.7. Nature. 2021;593(7857):130–35. doi:10.1038/s41586-021-03398-2. PMID: 33684923.
23. McCallum M, Bassi J, De Marco A, Chen A, Walls AC, Di Iulio J, Tortorici MA, Navarro MJ, Silacci-Fregni C, Saliba C, et al. SARS-CoV-2 immune evasion by the B.1.427/B.1.429 variant of concern. Sci. 2021;373(6555):648–54. doi:10.1126/science.abi7994. PMID: 34210893.
24. Chen RE, Winkler ES, Case JB, Aziati ID, Bricker TL, Joshi A, Darling TL, Ying B, Errico JM, Shrihari S, et al. In vivo monoclonal antibody efficacy against SARS-CoV-2 variant strains. Nature. 2021;596(7870):103–08. doi:10.1038/s41586-021-03720-y. PMID: 34153975.
25. Wang P, Casner RG, Nair MS, Wang M, Yu J, Cerutti G, Liu L, Kwong PD, Huang Y, Shapiro L, et al. Increased resistance of SARS-CoV-2 variant P.1 to antibody neutralization. Cell Host & Microbe. 2021;29(5):747–51 e744. doi:10.1016/j.chom.2021.04.007. PMID: 33887205.
26. Morris DH, Gostic KM, Pompei S, Bedford T, Luksza M, Neher RA, Grenfell BT, Lassig M, McCauley JW. Predictive modeling of influenza shows the promise of applied evolutionary biology. Trends Microbiol. 2018;26(2):102–18. doi:10.1016/j.tim.2017.09.004. PMID: 29097090.
27. Sun Y, Lin W, Dong W, Xu J. Origin and evolutionary analysis of the SARS-CoV-2 omicron variant. J Biosaf Biosecur. 2022;4 (1):33–37. doi:10.1016/j.jobb.2021.12.001. PMID: 35005525.
28. Alfaleh MA, Zawawi A, Al-Amri SS, Hashem AM. David versus goliath: ACE2-Fc receptor traps as potential SARS-CoV-2 inhibitors. MAbs. 2022;14(1):2057832. doi:10.1080/19420862.2022.2057832.
29. Lei C, Qian K, Li T, Zhang S, Fu W, Ding M, Hu S. Neutralization of SARS-CoV-2 spike pseudotyped virus by recombinant ACE2-Ig. Nat Commun. 2020;11(1):2070. doi:10.1038/s41467-020-16048-4. PMID: 32332765.
30. Tanaka S, Nelson G, Olson CA, Buzko O, Higashide W, Shin A, Gonzalez M, Taft J, Patel R, Buta S, et al. An ACE2 triple decoy that

neutralizes SARS-CoV-2 shows enhanced affinity for virus variants. null. 2021;11:12740. doi:10.1038/s41598-021-91809-9.

31. Guo L, Bi W, Wang X, Xu W, Yan R, Zhang Y, Zhao K, Li Y, Zhang M, Cai X, et al. Engineered trimeric ACE2 binds viral spike protein and locks it in "three-up" conformation to potently inhibit SARS-CoV-2 infection. Cell Res. 2021;31:98–100. doi:10.1038/s41422-020-00438-w. PMID: 33177651.

32. Miller A, Leach A, Thomas J, McAndrew C, Bentley E, Mattiuzzo G, John L, Mirazimi A, Harris G, Gamage N, et al. A super-potent tetramerized ACE2 protein displays enhanced neutralization of SARS-CoV-2 virus infection. null. 2021;11:10617. doi:10.1038/s41598-021-89957-z. PMID: 34012108.

33. Hunt AC, Case JB, Park YJ, Cao L, Wu K, Walls AC, Liu Z, Bowen JE, Yeh HW, Saini S, et al. Multivalent designed proteins protect against SARS-CoV-2 variants of concern. bioRxiv. 2021. doi:10.1101/2021.07.07.451375. PMID: 34268509.

34. Zhang L, Dutta S, Xiong S, Chan M, Chan KK, Fan TM, Bailey KL, Lindeblad M, Cooper LM, Rong L, et al. Engineered ACE2 decoy mitigates lung injury and death induced by SARS-CoV-2 variants. Nat Chem Biol. 2022. doi:10.1038/s41589-021-00965-6. PMID: 35046611.

35. Chan KK, Dorosky D, Sharma P, Abbasi SA, Dye JM, Kranz DM, Herbert AS, Procko E. Engineering human ACE2 to optimize binding to the spike protein of SARS coronavirus 2. Science. 2020;369:1261–65. doi:10.1126/science.abc0870. PMID: 32753553.

36. Cao L, Goreshnik I, Coventry B, Case JB, Miller L, Kozodoy L, Chen RE, Carter L, Walls AC, Park YJ, et al. De Novo design of picomolar SARS-CoV-2 miniprotein inhibitors. Science. 2020;370:426–31. doi:10.1126/science.abd9909. PMID: 32907861.

37. Xiao T, Lu J, Zhang J, Johnson RI, McKay LGA, Storm N, Lavine CL, Peng H, Cai Y, Rits-Volloch S, et al. A trimeric human angiotensin-converting enzyme 2 as an anti-SARS-CoV-2 agent. Nature Struct Molecul Biol. 2021;28:202–09. doi:10.1038/s41594-020-00549-3.

38. Linsky TW, Vergara R, Codina N, Nelson JW, Walker MJ, Su W, Barnes CO, Hsiang TY, Esser-Nobis K, Yu K, et al. De Novo design of potent and resilient hACE2 decoys to neutralize SARS-CoV-2. Sci. 2020;370:1208–14. doi:10.1126/science.abe0075. PMID: 33154107.

39. Patino-Galindo JA, Filip I, Chowdhury R, Maranas CD, Sorger PK, AlQuraishi M, Rabadan R. Recombination and lineage-specific mutations linked to the emergence of SARS-CoV-2. Genome Med. 2021;13:124. doi:10.1186/s13073-021-00943-6. PMID: 34362430.

40. Shang J, Ye G, Shi K, Wan Y, Luo C, Aihara H, Geng Q, Auerbach A, Li F. Structural basis of receptor recognition by SARS-CoV-2. Nature. 2020;581:221–24. doi:10.1038/s41586-020-2179-y. PMID: 32225175.

41. Wrapp D, Wang N, Corbett KS, Goldsmith JA, Hsieh CL, Abiona O, Graham BS, McLellan JS. Cryo-EM structure of the 2019-nCov spike in the prefusion conformation. Sci. 2020;367:1260–63. doi:10.1126/science.abb2507. PMID: 32075877.

42. Gutgsell AR, Gunnarsson A, Forssen P, Gordon E, Fornstedt T, Geschwindner S. Biosensor-enabled deconvolution of the avidity-induced affinity enhancement for the SARS-CoV-2 spike protein and ACE2 interaction. Anal Chem. 2022;94:1187–94. doi:10.1021/acs.analchem.1c04372. PMID: 34964599.

43. Imai M, Iwatsuki-Horimoto K, Hatta M, Loeber S, Halfmann PJ, Nakajima N, Watanabe T, Ujie M, Takahashi K, Ito M, et al. Syrian hamsters as a small animal model for SARS-CoV-2 infection and countermeasure development. Proc Natl Acad Sci U S A. 2020;117:16587–95. doi:10.1073/pnas.2009799117. PMID: 32571934.

44. Tamming LA, Duque D, Tran A, Zhang W, Pfeifle A, Laryea E, Wu J, Raman SNT, Gravel C, Russell MS, et al. DNA based vaccine expressing SARS-CoV-2 spike-CD40L fusion protein confers protection against challenge in a Syrian hamster model. Front Immunol. 2021;12:785349. doi:10.3389/fimmu.2021.785349. PMID: 35095861.

45. Mulka KR, Beck SE, Solis CV, Johanson AL, Queen SE, McCarron ME, Richardson MR, Zhou R, Marinho P, Jedlicka A, et al. Progression and resolution of severe acute respiratory syndrome coronavirus 2 (SARS-CoV-2) infection in golden Syrian hamsters. Am J Pathol. 2022;192:195–207. doi:10.1016/j.ajpath.2021.10.009. PMID: 34767812.

46. Gruber AD, Osterrieder N, Bertzbach LD, Vladimirova D, Greuel S, Ihlow J, Horst D, Trimpert J, Dietert K. Standardization of reporting criteria for lung pathology in SARS-CoV-2-infected hamsters: what matters? Am J Respir Cell Mol Biol. 2020;63:856–59. doi:10.1165/rcmb.2020-0280LE. PMID: 32897757.

47. Svilenov HL, Bester R, Sacherl J, Absmeier R, Peters C, Protzer U, Brockmeyer C, Buchner J. Multimeric ACE2-IgM fusions as broadly active antivirals that potently neutralize SARS-CoV-2 variants. Commun Biol. 2022;5:1237. doi:10.1038/s42003-022-04193-z. PMID: 36371561.

48. Campbell M. A conversation with Professor Josef Penninger on the journey to a COVID-19 therapeutic; 2020. https://www.technologynetworks.com/proteomics/blog/a-conversation-with-professor-josef-penninger-on-the-journey-to-a-covid-19-therapeutic-340785.

49. Monteil V, Kwon H, Prado P, Hagelkruys A, Wimmer RA, Stahl M, Leopoldi A, Garreta E, Hurtado Del Pozo C, Prosper F, et al. Inhibition of SARS-CoV-2 infections in engineered human tissues using clinical-grade soluble human ACE2. Cell. 2020;181:905–13 e907. doi:10.1016/j.cell.2020.04.004. PMID: 32333836.

50. Kuba K, Imai Y, Rao S, Gao H, Guo F, Guan B, Huan Y, Yang P, Zhang Y, Deng W, et al. A crucial role of angiotensin converting enzyme 2 (ACE2) in SARS coronavirus-induced lung injury. Nat Med. 2005;11:875–79. doi:10.1038/nm1267. PMID: 16007097.

51. Lovren F, Pan Y, Quan A, Teoh H, Wang G, Shukla PC, Levitt KS, Oudit GY, Al-Omran M, Stewart DJ, et al. Angiotensin converting enzyme-2 confers endothelial protection and attenuates atherosclerosis. Am J Physiol Heart Circ Physiol. 2008;295:H1377–1384. doi:10.1152/ajpheart.00331.2008. PMID: 18660448.

52. Khan A, Benthin C, Zeno B, Albertson TE, Boyd J, Christie JD, Hall R, Poirier G, Ronco JJ, Tidswell M, et al. A pilot clinical trial of recombinant human angiotensin-converting enzyme 2 in acute respiratory distress syndrome. Crit Care. 2017;21:234. doi:10.1186/s13054-017-1823-x. PMID: 28877748.

53. Zoufaly A, Poglitsch M, Aberle JH, Hoepler W, Seitz T, Traugott M, Grieb A, Pawelka E, Laferl H, Wenisch C, et al. Human recombinant soluble ACE2 in severe COVID-19. Lancet Respir Med. 2020;8:1154–58. doi:10.1016/S2213-2600(20)30418-5. PMID: 33131609.

54. Iwasaki A. Exploiting mucosal immunity for antiviral vaccines. Annu Rev Immunol. 2016;34:575–608. doi:10.1146/annurev-immunol-032414-112315. PMID: 27168245.

55. Hou YJ, Okuda K, Edwards CE, Martinez DR, Asakura T, Dinnon KH, Kato T, Lee RE, Yount BL, Mascenik TM, et al. SARS-CoV-2 reverse genetics reveals a variable infection gradient in the respiratory tract. Cell. 2020;182:429–46 e414. doi:10.1016/j.cell.2020.05.042. PMID: 32526206.

56. Wang W, Xu Y, Gao R, Lu R, Han K, Wu G, Tan W. Detection of SARS-CoV-2 in different types of clinical specimens. JAMA. 2020;323:1843–44. doi:10.1001/jama.2020.3786. PMID: 32159775.

57. Parray HA, Shukla S, Perween R, Khatri R, Shrivastava T, Singh V, Murugavelu P, Ahmed S, Samal S, Sharma C, et al. Inhalation monoclonal antibody therapy: a new way to treat and manage respiratory infections. Appl Microbiol Biotechnol. 2021;105:6315–32. doi:10.1007/s00253-021-11488-4. PMID: 34423407.

58. Ku Z, Xie X, Hinton PR, Liu X, Ye X, Muruato AE, Ng DC, Biswas S, Zou J, Liu Y, et al. Nasal delivery of an IgM offers broad protection from SARS-CoV-2 variants. Nature. 2021;595:718–23. doi:10.1038/s41586-021-03673-2. PMID: 34082438.

59. Halwe S, Kupke A, Vanshylla K, Liberta F, Gruell H, Zehner M, Rohde C, Krahling V, Gellhorn Serra M, Kreer C, et al. Intranasal administration of a monoclonal neutralizing antibody protects mice against SARS-CoV-2 infection. Viruses. 2021;13. doi:10.3390/v13081498. PMID: 34452363.

60. Fu YM, Singh A, Lim R, Ledesma A, Lee D, Rivero-Nava L, Ko J, Rivera I, Sattler RA, Manning JT, et al. Protective effects of STI-2020 antibody delivered post-infection by the intranasal or intravenous route in a Syrian golden hamster COVID-19 model. bioRxiv. 2020. doi:10.1101/2020.10.28.359836.

61. Urano E, Itoh Y, Suzuki T, Sasaki T, Kishikawa JI, Akamatsu K, Higuchi Y, Sakai Y, Okamura T, Mitoma S, et al. An engineered ACE2 decoy broadly neutralizes omicron subvariants and shows therapeutic effect in SARS-CoV-2-infected cynomolgus macaques. bioRxiv. 2023. doi:10.1101/2022.12.29.522275.

62. Makela AR, Ugurlu H, Hannula L, Kant R, Salminen P, Fagerlund R, Maki S, Haveri A, Strandin T, Kareinen L, et al. Intranasal trimeric sherpa body inhibits SARS-CoV-2 including recent immunoevasive omicron subvariants. Nat Commun. 2023;14:1637. doi:10.1038/s41467-023-37290-6. PMID: 36964125.

63. Bar-On YM, Flamholz A, Phillips R, Milo R. SARS-CoV-2 (COVID-19) by the numbers. Elife. 2020;9. doi:10.7554/eLife.57309. PMID: 32228860.

64. Li JZ, Aga E, Bosch RJ, Pilkinton M, Kroon E, MacLaren L, Keefer M, Fox L, Barr L, Acosta E, et al. Time to viral rebound after interruption of modern antiretroviral therapies. Clin Infect Dis. 2022;74:865–70. doi:10.1093/cid/ciab541. PMID: 34117753.

65. Boucau J, Uddin R, Marino C, Regan J, Flynn JP, Choudhary MC, Chen G, Stuckwisch AM, Mathews J, Liew MY, et al. Characterization of virologic rebound following nirmatrelvir-ritonavir treatment for COVID-19. Clin Infect Dis. 2022. doi:10.1093/cid/ciac512. PMID: 35737946.

66. Ranganath N, O'Horo JC, Challener DW, Tulledge-Scheitel SM, Pike ML, Michael O'Brien R, Razonable RR, Shah A. Rebound phenomenon after nirmatrelvir/ritonavir treatment of coronavirus disease-2019 in high-risk persons. Clin Infect Dis. 2022. doi:10.1093/cid/ciac481. PMID: 35698452.

67. Baum A, Ajithdoss D, Copin R, Zhou A, Lanza K, Negron N, Ni M, Wei Y, Mohammadi K, Musser B, et al. REGN-COV2 antibodies prevent and treat SARS-CoV-2 infection in rhesus macaques and hamsters. Sci. 2020;370:1110–15. doi:10.1126/science.abe2402. PMID: 33037066.

68. Keyt BA, Baliga R, Sinclair AM, Carroll SF, Peterson MS. Structure function, and therapeutic use of IgM antibodies. Antibodies. 2020;9:53. doi:10.3390/antib9040053. PMID:

69. Gagnon P, Hensel F, Lee S, Zaidi S. Chromatographic behavior of IgM: dNA complexes. J Chromatogr A. 2011;1218:2405–12. doi:10.1016/j.chroma.2010.12.066. PMID: 21215402.

70. Sama IE, Voors AA, van Veldhuisen DJ. New data on soluble ACE2 in patients with atrial fibrillation reveal potential value for treatment of patients with COVID-19 and cardiovascular disease. Eur Heart J. 2020;41:4047–49. doi:10.1093/eurheartj/ehaa761. PMID: 33118012.

71. Wallentin L, Lindback J, Eriksson N, Hijazi Z, Eikelboom JW, Ezekowitz MD, Granger CB, Lopes RD, Yusuf S, Oldgren J, et al. Angiotensin-converting enzyme 2 (ACE2) levels in relation to risk factors for COVID-19 in two large cohorts of patients with atrial fibrillation. Eur Heart J. 2020;41:4037–46. doi:10.1093/eurheartj/ehaa697. PMID: 32984892.

72. Glasgow A, Glasgow J, Limonta D, Solomon P, Lui I, Zhang Y, Nix MA, Rettko NJ, Zha S, Yamin R, et al. Engineered ACE2 receptor traps potently neutralize SARS-CoV-2. Proc Natl Acad Sci U S A. 2020;117:28046–55. doi:10.1073/pnas.2016093117. PMID: 33093202.

73. Borrok MJ, Luheshi NM, Beyaz N, Davies GC, Legg JW, Wu H, Dall'acqua WF, Tsui P. Enhancement of antibody-dependent cell-mediated cytotoxicity by endowing IgG with FcalphaRI (CD89) binding. MAbs. 2015;7:743–51. doi:10.1080/19420862.2015.1047570. PMID: 25970007.

74. Von Kreudenstein TS, Escobar-Carbrera E, Lario PI, D'Angelo I, Brault K, Kelly J, Durocher Y, Baardsnes J, Woods RJ, Xie MH, et al. Improving biophysical properties of a bispecific antibody scaffold to aid developability: quality by molecular design. MAbs. 2013;5:646–54. doi:10.4161/mabs.25632. PMID: 23924797.

75. Weinreich DM, Sivapalasingam S, Norton T, Ali S, Gao H, Bhore R, Xiao J, Hooper AT, Hamilton JD, Musser BJ, et al. REGEN-COV antibody combination and outcomes in outpatients with covid-19. N Engl J Med. 2021;385:e81. doi:10.1056/NEJMoa2108163. PMID: 34587383.

76. Nathan R, Shawa I, De La Torre I, Pustizzi JM, Haustrup N, Patel DR, Huhn G. A narrative review of the clinical practicalities of bamlanivimab and etesevimab antibody therapies for SARS-CoV-2. Infect Dis Ther. 2021;10:1933–47. doi:10.1007/s40121-021-00515-6. PMID: 34374951.

77. Corman VM, Landt O, Kaiser M, Molenkamp R, Meijer A, Chu DK, Bleicker T, Brunink S, Schneider J, Schmidt ML, et al. Detection of 2019 novel coronavirus (2019-nCov) by real-time RT-PCR. Euro Surveill. 2020;25. doi:10.2807/1560-7917.ES.2020.25.3.2000045. PMID: 31992387.

78. Akache B, Renner TM, Tran A, Deschatelets L, Dudani R, Harrison BA, Duque D, Haukenfrers J, Rossotti MA, Gaudreault F, et al. Immunogenic and efficacious SARS-CoV-2 vaccine based on resistin-trimerized spike antigen SmT1 and SLA archaeosome adjuvant. null. 2021;11:21849. doi:10.1038/s41598-021-01363-7. PMID: 34750472.